dilution of validated sources of 20 or 1456 ppmv HA with N_2 by using calibrated flow controllers. Gaseous streams of $(H_3CO)_2POCH_3$ were prepared by similar methods from a saturated vapor of $(H_3CO)_2POCH_3$ at 20°C.

33. R. M. Crooks, H. C. Yang, L. J. McEllistrem, R. C. Thomas, A. J. Ricco, *Faraday Discuss.* **107**, 285 (1997).
34. R. Berger *et al.*, *Science*, **276**, 2021 (1997).
35. J. Fritz *et al.*, *Science* **288**, 316 (2000).
36. D. T. McQuade, A. E. Pullen, T. M. Swager, *Chem. Rev.* **100**, 2537 (2000).
37. M. R. Dawood, R. Allan, K. Fowke, J. Embree, G. W. Hammond, *J. Clin. Microbiol.* **30**, 2279 (1992).
38. T. Vo-Dinh, D. L. Stokes, *Field Anal. Chem. Technol.* **3**, 346 (1999).
39. M. Niculescu *et al.*, *Anal. Chem.* **72**, 1591 (2000).
40. R. R. Shah, N. L. Abbott, *J. Am. Chem. Soc.* **121**, 11300 (1999).
41. A. E. Martell, M. Calvin, *Chemistry of Metal Chelate Compounds* (Prentice-Hall, New York, 1952).
42. R. R Shah, N. L. Abbott, *J. Phys. Chem B* **105**, 4936 (2001).
43. Y. Marcus, *J. Chem. Soc. Dalton Trans.* 2265 (1991).
44. J. F. Coetzee, W. R Sharpe, *J. Solution Chem.* **1**, 77 (1972).
45. Supported in part by the National Science Foundation (grants CTS-9502263 and DMR-0079983) and Office of Naval Research (Presidential Early Career Award for Scientists and Engineers to N.L.A.). N.L.A. thanks Y.-Y. Luk (University of Wisconsin) for helpful discussions.

7 May 2001; accepted 23 July 2001

Ring Closure of Carbon Nanotubes

Masahito Sano,* Ayumi Kamino, Junko Okamura, Seiji Shinkai

Lightly etched single-walled carbon nanotubes are chemically reacted to form rings. The rings appear to be fully closed as opposed to open coils, as ring-opening reactions did not change the structure of the observed rings. The average diameter of the rings was 540 nanometers with a narrow size distribution. The nanotubes in solution were modeled as wormlike polymer chains, yielding a persistence length of 800 nanometers. Nanotubes shorter than this length behave stiffly and stay nearly straight in solution. However, nanotubes longer than the Kuhn segment length of 1600 nanometers undergo considerable thermal fluctuation, suggesting a greater flexibility of these materials than is generally assumed.

With currently available synthetic methods (*1, 2*), carbon nanotubes are always grown as long strings, and this string shape is largely responsible for their immediate applications to field emission source (*3*), probe tips (*4, 5*), tweezers (*6*), molecular or chemical wires (*7, 8*), and fibrous composites (*9*). Despite their importance, however, there has been no effective means to shape a large number of individual carbon nanotubes in a controlled way. Chemical modification of nanotubes along logically designed pathways may be one such method. In particular, ring-forming reactions yield a result that can be easily confirmed by microscopic techniques. So far, accidental occurrences of ring structures during nanotube syntheses have been reported (*10, 11*). There is also a report of ring formation by physical coiling (*12*). We show that covalent ring-closure reactions applied to commercially available carbon nanotubes produce a sizable number of ring-shaped tubes where the tubes bond only to themselves. The rings show a narrow size distribution, which we explain by modeling the nanotubes in solution as wormlike polymer chains. The analysis gives a characteristic length scale, which classifies a given nanotube as either stiff or semiflexible in solution. Such a scale is useful for understanding aggregation behaviors, such as bundle formations, and designing chemical modifications of nanotubes.

Commercially available pristine single-walled carbon nanotubes (SWNTs) are generally too long to be dispersed in solution and have no well-defined chemical functional groups to modify. Ultrasonicating SWNTs in concentrated H_2SO_4/HNO_3 is known to cut SWNTs into many short pieces (*13*). Because scission occurs preferably at defect sites, this treatment produces a broad distribution of open-ended SWNTs. The cut SWNTs are then etched lightly in H_2SO_4/H_2O_2 to afford oxygen-containing groups at both ends, of which some are phenolic hydroxides and carboxylic acids (*14*). The resulting SWNTs can be dispersed relatively well in water and dimethylformamide (DMF), although some tend to aggregate into bundles even in these dispersions. We note that dispersible amounts of SWNTs in various solvents (*15, 16*) depend on history of chemical treatments as well as lengths.

Ring closure can be achieved with a number of organic reactions with the oxygen-containing groups at the tube ends, provided that SWNTs have not completely collapsed or coagulated at each step of the procedure. Any processes that promote aggregation, such as filtering, should be avoided as much as possible. A possible scheme with 1,3-dicyclohexylcarbodiimide (DCC) is illustrated in Fig. 1. Raman shift of the A_{1g} mode (*17*) indicates that SWNTs (laser-oven products purchased from Rice University) have a diameter of 1.2 nm. Large aggregates of SWNTs after the acid treatments were removed by ultracentrifuge at $3500g$. The remaining SWNTs in the supernatant solution were dispersed in dry DMF so that the solution was lightly colored and an excess amount of DCC was added. The mixture was stirred overnight at room temperature, after which solid materials were collected and washed on a Teflon filter. For the following statistical analysis, the reaction mixture before filtration (Fig. 2A) was used for sampling. Another reaction by modifying carboxylic acids to acid chlorides (*13, 18*) also produced rings but with lower yields, probably because of poorer dispersion of acid chloride SWNTs in DMF.

Atomic force microscopy (AFM) reveals rings of an average diameter of 540 nm or equivalently a contour length of 1.7 μm (Fig. 2B). A control sample of acid-treated SWNTs without reaction also produces a ring-shaped feature that is caused by physical coiling. This happens rarely, and only one or two loops, if any, are seen in the area, as shown in Fig. 2A. The diameter of coils obtained by Martel *et al.* (*12*) is larger on average, which may be due to the fact that the coils are open-ended whereas the present rings are closed. Once formed, rings are quite stable both chemically and physically. Ring-opening reactions, such as treating rings with dimethylaminopyridine and *n*-butylamine or NaOH, had no effect on the rings. Heating rings to 500°C under N_2 atmosphere for 3 hours did not open the rings. Because any oxygen-containing organic bonds should have decomposed at this temperature, it is interesting to investigate the nature of the linkage after the heat treatment.

During reproducibility experiments, we noticed that the size of rings was roughly the same even when different chemical conditions, such as water contents and different functional groups, were used. Figure 3A shows a histogram of contour lengths of rings measured directly from AFM images. There are very few rings with the contour lengths below 1.3 μm and above 2.1 μm. To explain this narrow distribution, it is necessary to understand properties of SWNTs in the reaction mixture, i.e., under what conditions two ends of a SWNT can meet by thermal fluctuation. Here, we model SWNTs in DMF by wormlike polymer chains with excluded vol-

---

Chemotransfiguration Project–JST, Kurume, Fukuoka 839-0861, Japan.

*To whom correspondence should be addressed.

ume effects. The wormlike chain is a statistical mechanical model often used for a stiff polymer (*19*). A measure of elastic stiffness is given by a persistence length, p. When the contour length of a chain, L, is small compared with p, the chain is considered stiff. To obtain ring-closure probability $G(L;p)$ of wormlike chains in Yamakawa-Stockmayer theory, a distribution function of the end-to-end distance vector is solved within a perturbation framework. Ring closure is achieved by letting the end-to-end distance to zero. Finally, integrating over all possible angles at which two chain ends meet yields the result (*20*)

$$G(L;p) \begin{cases} 496.51r^{-1}e^{-7.0266/r}(1-0.81242r) & \text{for } r < 0.96093 \\ 0.32992r^{-1.5}(1-0.625r^{-1}- 0.12344r^{-2}) & \text{for } r > 0.96093 \end{cases} \qquad (1)$$

where $r = L/2p$ is the reduced length. Thus, G is completely determined by a given material parameter p. It is nearly zero for $L < 1.5p$ and becomes significant only for $L > 2p$. If $W(L)$ denotes the contour length distribution of acid-treated SWNTs in DMF before the reaction, the ring contour length follows a joint distribution $W(L)G(L;p)$. In reality, W is not directly accessible and must be estimated.

Figure 3B plots a histogram of contour lengths of all tubes in a control sample without reaction. The tube lengths were measured directly from AFM images of cast films after evaporating DMF. If W is approximated (after proper normalization) by the histogram given in Fig. 3B, the least squares fit of the observed ring-contour distribution (a normalized histogram in Fig. 3A) by WG yields $p = 0.82$ μm. The corresponding best fit curves WG and G are displayed as solid curves in Fig. 3, A and B, respectively. AFM images indicate that longer tubes tend to be thicker, and nearly all tubes with lengths longer than 1 μm are bundles. Because some SWNTs are likely to be aggregated into bundles during solvent evaporation, W probably takes larger values at shorter lengths and decays faster at longer lengths than the histogram suggests. Because G stays very small at short L, this uncertainty in estimating W is not relevant. Other control samples produce histograms that shear the common features of having a maximum at small L and a decaying tail at longer L, but with different peak positions and decaying rates. All of them give p in the range 0.80 ± 0.05 μm. This is consistent with p being a material property that should not depend on a choice of W. The numerical reasons of insensitivity of p on W are that, as long as W decays to zero by about 2 μm, p is mainly determined by the left-hand shoulder of the ring contour distribution and the effects of W appear only on the fit over the right-hand shoulder. Because a bundle length defines a maximum length of individual SWNTs within the bundle, both individual SWNTs and bundles satisfy this condition. A helical wormlike chain model (*21*) to represent G gives a p similar to that of the wormlike chain model. The value of $p = 0.8$ μm is comparable to the stiffest polymer chains reported so far, such as DNA and cellulose derivatives (*22*). This means that, despite its large Young's modulus of about 1 TPa (*23*), thermal fluctuation can bend a SWNT like a semiflexible polymer if its contour length exceeds the Kuhn statistical segment length of $2p = 1.6$ μm.

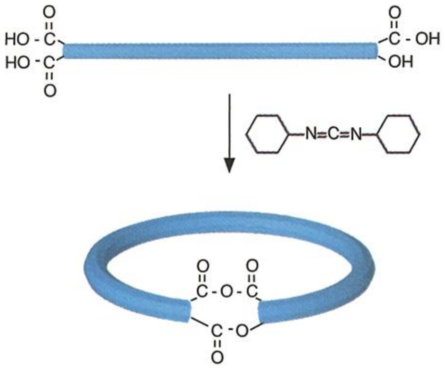

Fig. 1. A possible scheme for the ring-closure reaction with DCC.

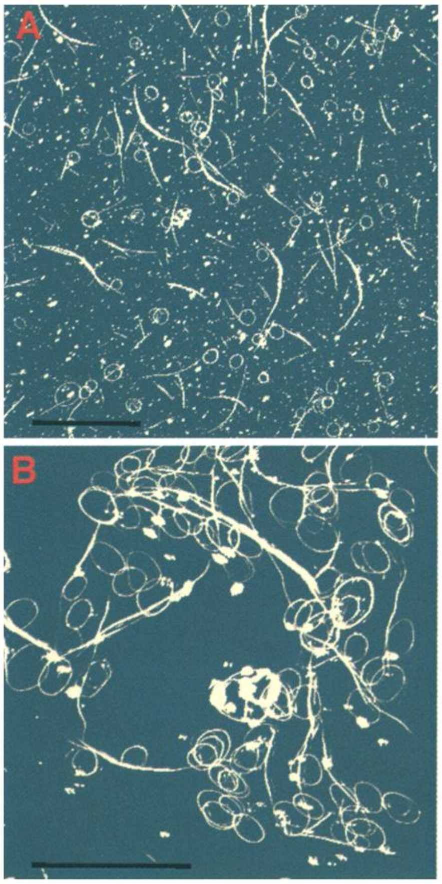

Fig. 2. AFM images of carbon nanotube rings cast on mica. **(A)** A reaction mixture without any purification. Each ring is dispersed well and is not a part of a long tube. Scale bar, 5 μm. **(B)** A reaction mixture after washing and filtering through 0.8-μm Teflon filer. Rings appear to stick to each other after these processes. Scale bar, 2 μm.

When only the acid-treated SWNTs with lengths shorter than 1 μm were used, few rings formed. The ring-contour histogram shown in Fig. 3A is not multimodal. These observations indicate that rings result from the ring-closure reaction of a single tube, rather than the closing of oligomerically linked tubes that have been polymerized linearly by bimolecular reactions. At least two factors are responsible for predominant closure reactions that are usually unfavorable in ordinary reactions. The concentrations of SWNTs were extremely low. Absorption spectroscopy indicates that the lightly colored solution contains less than 0.05 mg/ml. An AFM image (Fig. 2A) also shows that the molar concentration is so low that the number of tubes is

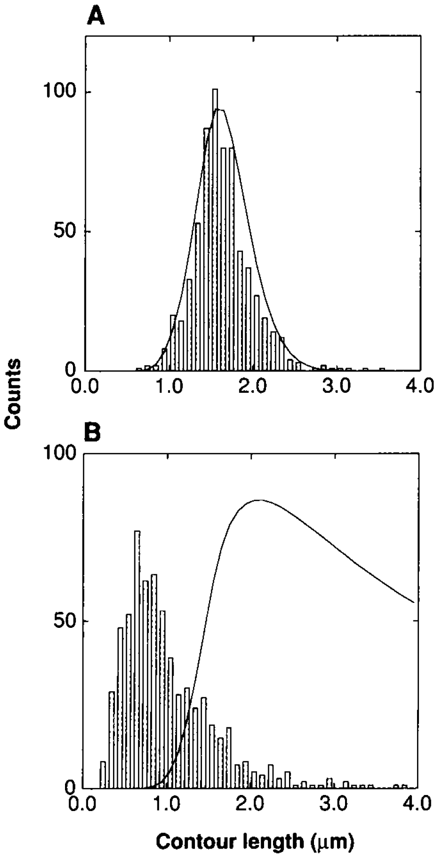

Fig. 3. Statistical analysis of ring size. A small drop of the reaction mixture was cast on mica and DMF was evaporated. The contour lengths were measured directly from AFM images of these cast films. **(A)** A histogram of contour lengths of rings. The solid curve is the best fit joint distribution function $W(L)G(L;p) = 0.82$ μm. **(B)** A histogram of contour lengths of all tubes without reaction. $W(L)$ was obtained from a smooth curve enveloping the histogram. The solid curve is the best fit ring-closure probability distribution $G(L;\ p = 0.82$ μm).

almost countable. Ordinary reactions under an effectively low concentration condition are known to produce polymer rings, such as syntheses of cyclic peptides on an oxime resin (*24*). Also, dynamic light scattering yields a diffusion constant of 4×10^{-8} cm^2/s for even very short SWNTs. This value is 10^2 to 10^3 times slower than typical organic molecules in solution. Thus, bimolecular collision is highly suppressed, whereas intramolecular reaction is not affected. This implies that *W* does not shift to the right during reaction under the present conditions.

Height examinations of the rings in the AFM images show that some rings are thicker than a few nm, implying rings of bundles. Either postaggregation of linear SWNTs onto a single-tube ring or ring closure of a single bundle forms ring-shaped bundles during reaction. It is difficult to verify from AFM images, because the former case may take place also during solvent evaporation. The good fit over the left-hand shoulder of the ring distribution by a single value of *p* suggests the former case, whereas the fine fit over the right-hand shoulder by the all-tubes distribution of Fig. 3B favors the latter. Unless *p* depends significantly on a number of individual SWNTs in a bundle, rings can contain both types. For possible controls of the average ring size, it is interesting to see if *p* depends on the SWNT diameter.

References

1. R. Saito, G. Dresselhaus, M. S. Dresselhaus, *Physical Properties of Carbon Nanotubes* (Imperial College, London, 1998).
2. A. G. Rinzler *et al.*, *Appl. Phys. A* **67**, 29 (1998).
3. W. A. de Heer, A. Châtelain, D. Ugarte, *Science* **270**, 1179 (1995).
4. H. Dai, J. H. Hafner, A. G. Rinzler, D. T. Colbert, R. E. Smalley, *Nature* **384**, 147 (1996).
5. S. S. Wong, E. Joselevich, A. T. Woolley, C. L. Cheung, C. M. Lieber, *Nature* **394**, 52 (1998).
6. P. Kim, C. M. Lieber, *Science* **286**, 2148 (1999).
7. T. Rueckes *et al.*, *Science* **289**, 94 (2000).
8. J. Kong *et al.*, *Science* **287**, 622 (2000).
9. B. Vigolo *et al.*, *Science* **290**, 1331 (2000).
10. J. Liu *et al.*, *Nature* **385**, 780 (1997).
11. M. Ahlskog *et al.*, *Chem. Phys. Lett.* **300**, 202 (1999).
12. R. Martel, H. R. Shea, P. Avouris, *Nature* **398**, 299 (1999).
13. J. Liu *et al.*, *Science* **280**, 1253 (1998).
14. J. L. Bahr, E. T. Mickelson, M. J. Bronikowski, R. E. Smalley, J. M. Tour, *Chem. Commun.* **2001**, 193 (2001).
15. A. Kuznetsova *et al.*, *Chem. Phys. Lett.* **321**, 292 (2000).
16. K. D. Ausman, R. Piner, O. Lourie, R. S. Ruoff, *J. Phys. Chem. B* **104**, 8911 (2000).
17. R. Saito, T. Takeya, T. Kimura, G. Dresselhaus, M. S. Dresselhaus, *Phys. Rev. B* **57**, 4145 (1998).
18. J. Chen *et al.*, *Science* **282**, 95 (1998).
19. P. J. Flory, *Statistical Mechanics of Chain Molecules* (Wiley, New York, 1969), pp. 401–403.
20. H. Yamakawa, W. H. Stockmayer, *J. Chem. Phys.* **57**, 2843 (1972).
21. J. Shimada, H. Yamakawa, *Macromolecules* **17**, 689 (1984).
22. J. Brandrup, E. H. Immergut, *Polymer Handbook* (Wiley, New York, ed. 3, 1989).
23. M-F. Yu, B. S. Files, S. Arepalli, R. S. Ruoff, *Phys. Rev. Lett.* **84**, 5552 (2000).
24. H. Ishida, Z. Qi, M. Sokabe, K. Donowaki, Y. Inoue, *J. Org. Chem.* **66**, 2978 (2001).

26 March 2001; accepted 12 July 2001

Atlantic Water Flow Pathways Revealed by Lead Contamination in Arctic Basin Sediments

Charles Gobeil,[1]* Robie W. Macdonald,[2] John N. Smith,[3] Luc Beaudin[1]

Contaminant lead in sediments underlying boundary currents in the Arctic Ocean provides an image of current organization and stability during the past 50 years. The sediment distributions of lead, stable lead isotope ratios, and lead-210 in the major Arctic Ocean basins reveal close coupling of the Eurasian Basin with the North Atlantic during the 20th century. They indicate that the Atlantic water boundary current in the Eurasian Basin has been a prominent pathway, that contaminant lead from the Laptev Sea supplies surface water in the transpolar drift, and that the Canadian and Eurasian basins have been historically decoupled.

The close connection between the Arctic Ocean and contaminants released to the south is well documented (*1*). Although the atmosphere can transport volatile and particulate substances into the Arctic within days, over a longer time period the oceans may become the more important pathway (*1*, *2*). Pb provides one of the clearest examples of human activities that have overwhelmed natural cycles, particularly in the North Atlantic (*3–5*). Owing to its strong affinity for particles, Pb has a short residence time in surface waters (<5 years), and contamination there is mirrored in sediments of the underlying deep basins (*6*, *7*). Because the stable Pb isotope composition varies with source, the isotopic ratios can provide an incisive indicator of pathways impacted by humans (*8*).

Here, we examine sediment cores collected from the Arctic Ocean and Greenland Sea basins for evidence of contaminant Pb. Using the contaminant Pb inventory and its isotopic composition, we infer the source of the Pb and its pathways referring to present schemes of ocean current structure and ice drift (*9*, *10*). In the abyssal ocean, where sedimentation may be less than 1 mm per thousand years and where foragers often mix the top few cm of the sediments, contaminant Pb inputs are observed as increased Pb burden in a shallow surface mixed layer (SML). With a half-life of 22.3 years, excess ^{210}Pb in the sediments, i.e., ^{210}Pb deposited from the water as opposed to that produced by ^{226}Ra decay within the sediments, is an ideal indicator of the SML where the Pb deposited over the past 100 years resides. Detection of contaminant Pb above a variable background can be considerably reinforced with stable Pb isotope compositions because contaminant Pb usually differs from natural Pb (*8*), and the isotopic composition is little affected by kinetic processes occurring between source and sink. To identify contaminant Pb in Arctic basin sediments that accumulate slowly (*11*), we use three rigorous criteria: (i) There must be a SML enriched in ^{210}Pb. (ii) The concentration of Pb must be higher in the SML than in the sediments below. (iii) The stable Pb isotope composition must differ between the SML and the deeper sediments.

Sediment box cores were collected in 1994 at depths of 2265 to 4230 m in the Canadian, Eurasian, and Greenland Sea basins (Fig. 1); they were sectioned into 1-cm slices for the top 10 cm and then analyzed. All cores exhibit well-defined SMLs in the top 2 to 4 cm on the basis of the ^{210}Pb profiles (Fig. 1). In the Eurasian Basin, Pb concentrations in the SML are 1.6 to 4.8 μg g^{-1} higher than in the sediments immediately below, and the stable isotope ratios are lower. At stations 39 and 37, the shift in the isotopic composition associated with the change in Pb concentration in the SML is larger than at stations 36 and 35. In the Canadian Basin sediments, elevated ^{210}Pb activities in surface sediments are similar to those observed in the Greenland Sea and Eurasian basins, confirming an active scavenging of ^{210}Pb from the water column. However, at stations 26 and 11, Pb concentration does not differ between the SML and the sediments immediately below, and the stable Pb isotope ratios remain invariant

---

[1] Institut Maurice-Lamontagne, Mont-Joli, QC, G5H 3Z4, Canada. [2] Institute of Ocean Sciences, Sidney, BC, V8L 4B2, Canada. [3] Bedford Institute of Oceanography, Dartmouth, NS, B2Y 4A2, Canada.

*To whom correspondence should be addressed. E-mail: GobeilC@dfo-mpo.gc.ca